Structural, magnetic, and electrical studies on polycrystalline transition-metal-doped $BiFeO_3$ thin films

2009 J. Phys.: Condens. Matter 21 036001

(http://iopscience.iop.org/0953-8984/21/3/036001)

J. Phys.: Condens. Matter **21** (2009) 036001 (6pp) doi:10.1088/0953-8984/21/3/036001

Structural, magnetic, and electrical studies on polycrystalline transition-metal-doped $BiFeO_3$ thin films

P Kharel[1], S Talebi[1,2], B Ramachandran[3], A Dixit[1], V M Naik[2], M B Sahana[1], C Sudakar[1], R Naik[1], M S R Rao[3] and G Lawes[1]

[1] Department of Physics and Astronomy, Wayne State University, Detroit, MI 48201, USA
[2] Department of Natural Sciences, University of Michigan Dearborn, Dearborn, MI 48128, USA
[3] Department of Physics and Nano Functional Materials Technology Centre, Indian Institute of Technology Madras, Chennai 600036, India

Received 11 August 2008, in final form 9 November 2008
Published 11 December 2008
Online at stacks.iop.org/JPhysCM/21/036001

Abstract

We have synthesized a range of transition-metal-doped $BiFeO_3$ thin films on conducting silicon substrates using a spin-coating technique from metal–organic precursor solutions. Bismuth, iron and transition-metal–organic solutions were mixed in the appropriate ratios to produce 3% transition-metal-doped samples. X-ray diffraction studies show that the samples annealed in a nitrogen atmosphere crystallize in a rhombohedrally distorted $BiFeO_3$ structure with no evidence for any ferromagnetic secondary phase formation. We find evidence for the disappearance of the 404 cm^{-1} Raman mode for certain dopants indicative of structural distortions. The saturation magnetization of these $BiFeO_3$ films has been found to increase on doping with transition metal ions, reaching a maximum value of 8.5 emu cm^{-3} for the Cr-doped samples. However, leakage current measurements find that the resistivity of the films typically decreases with transition metal doping. We find no evidence for any systematic variation of the electric or magnetic properties of $BiFeO_3$ depending on the transition metal dopant, suggesting that these properties are determined mainly by extrinsic effects arising from defects or grain boundaries.

1. Introduction

Magnetoelectric multiferroics, which exhibit simultaneous magnetic and ferroelectric order, have been widely studied in recent years because of potential applications for developing novel storage media and spintronic devices [1]. Although several single-phase magnetoelectric multiferroics have been identified [1–5], $BiFeO_3$ is the only material presently known to express coupling between magnetic and ferroelectric order at room temperature [6]. The coexistence of a large ferroelectric polarization, comparable to those in $BaTiO_3$ and $PbTiO_3$, and the robust ferromagnetic moment reported in high quality $BiFeO_3$ thin films [7] has made this system especially promising for applications. However, the relatively modest magnetization and large leakage currents observed in many $BiFeO_3$ samples limit device applications for this material.

It has been suggested that the conductivity in $BiFeO_3$ may be strongly affected by the reduction of Fe^{3+} to Fe^{2+} [8]. Attempts have been made to lower the leakage current density by substituting Bi^{3+} with La^{3+} and Nd^{3+} [9]. It is thought that vacancies created by the removal of Bi^{3+} ions are compensated by the substitution of rare earth ions, reducing the conductivity. Replacing Fe^{3+} ions with other transition metal ions such as Cr^{3+} [10–12], Ti^{4+} [13–15], Mn^{3+} [16] and Sc^{3+} [17] that have better electrical stability is expected to increase the resistance by reducing valence fluctuations in Fe^{3+}. Conversely, substituting Ni^{2+} ions increases the leakage current [15]. Additionally, doping $BiFeO_3$ with magnetic transition metals has been observed to affect the magnetic properties [12, 13]. By conducting a systematic study of the effect of 3d transition metal doping on the structural, magnetic and electrical properties of $BiFeO_3$ we hope to clarify the mechanisms through which these dopants affect the characteristic behavior. Very recently, a similar study on $BiFeO_3$ films doped with Cr, Mn, Co, Ni and Cu has found that the saturation magnetization and leakage current can be improved for certain dopants [18], although the origin of these effects remains unclear.

2. Experimental details

The precursor solution for the pure $BiFeO_3$ samples was prepared by homogeneously mixing bismuth 2-ethylhexanoate and iron(III) 2-ethylhexanoate liquids in 1:1 ratio by the number of atoms. Similar metal–organic liquids were used to replace 3% Fe atoms in $BiFeO_3$ by Ti, V, Cr, Mn, Co, Ni, Cu and Zn. The Cr was added in the 3+ valence state, the Ti was added in the 4+ valence state, while the Mn, Ni, Co, Cu and Zn were added in the 2+ state. The solution was dispensed onto a conducting silicon (100) substrate, which was spun at 5000 rpm for 15 s, then baked at 550 °C for 90 s to remove the organic constituents. This process was repeated several times to build up the desired thickness of ≈1 μm. These samples were annealed at temperatures from 550 to 600 °C for 1 h in a nitrogen environment. We investigated the crystal structure using powder x-ray diffraction (XRD) on a Rigaku RU2000 diffractometer and the Fe valence with x-ray photoelectron spectroscopy (XPS) using Al Kα radiation. We probed the vibrational spectra of the samples by Raman spectroscopy using a 7–10 mW 514.5 nm Ar-ion laser line with a Renishaw 1000 micro Raman system having a 20 μm beam size in the backscattering geometry $[z(x+y, x+y)\bar{z}]$. Spectra were collected for 30 s at several different spots on each sample. The magnetic properties were characterized using a Quantum Design SQUID magnetometer and electrical properties were analyzed using a radiant ferroelectric analyzer. We confirmed that the samples had the expected doping levels using SEM EDX.

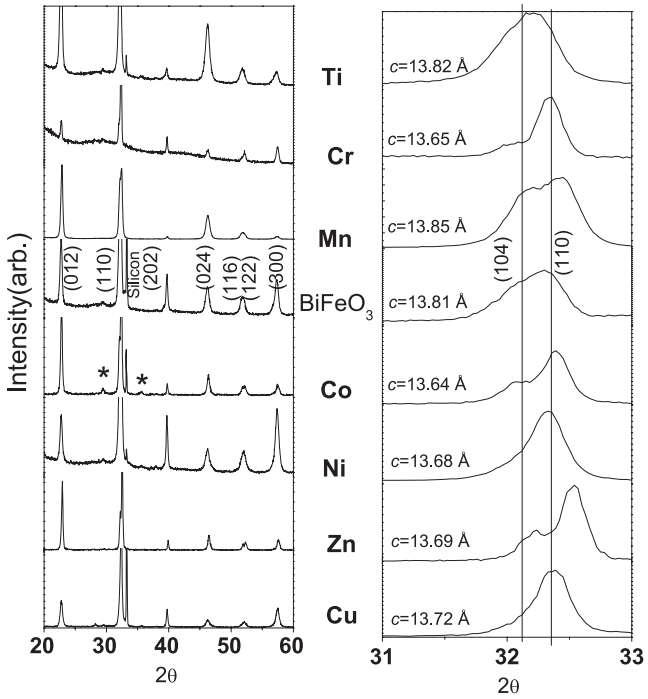

Figure 1. (a) X-ray diffraction pattern for undoped and TM-doped $BiFeO_3$ thin films. All peaks can be indexed to the rhombohedrally distorted $BiFeO_3$ structure. Peaks indicated by asterisks correspond to the $Bi_2Fe_4O_9$ secondary phase. The label for each panel indicates the transition metal dopant added to each $BiFeO_3$ sample. (b) XRD spectra close to $2\theta = 32°$ for the different samples. We have also given the c-axis parameter for each sample estimated by refining the XRD patterns.

3. Results and discussion

The $BiFeO_3$ crystal lattice is rather complex [19], since it exhibits a number of structural distortions [20]. The ideal perovskite lattice, with space group $Pm\bar{3}m$, can be distorted by Fe and Bi displacements to give a lattice with $R3m$ symmetry, or by rotations of the oxygen octahedra to give $R\bar{3}c$ symmetry. The combination of both of these distortions produces the ferroelectric $R3c$ structure. It has been suggested that the high temperature paraelectric structure for $BiFeO_3$ is $R\bar{3}c$ [20]. As shown in figure 1(a), the XRD patterns of the pure and TM-doped samples can be completely indexed to the rhombohedrally distorted $BiFeO_3$ structure with the space group $R3c$. Although most of the samples are single phase with the $BiFeO_3$ structure, a secondary phase can be seen in the V- and Co-doped films, consistent with reports on Sc-doped thin films [17]. This secondary phase, indicated by asterisks, is identified as $Bi_2Fe_4O_9$. We determined the grain size in the undoped $BiFeO_3$ film to be ≈17 nm using the Debye–Scherrer equation, while the grain size for the doped samples ranged from 16 to 39 nm.

The XRD patterns near $2\theta = 32°$ are shown in figure 1(b). The (104) and (110) peaks are overlapping, but can be distinguished in pure $BiFeO_3$. These peaks shift with Zn, Co, Mn and Cr substitution and overlap completely to give a single broad peak when Ni, Ti and Cu atoms are substituted for Fe. We find that the c-axis parameter depends on the dopant ion and is smallest for the Cr- and Co-doped films. The value for undoped $BiFeO_3$, $c = 13.81$ Å, is relatively close to the literature value, $c = 13.86$ Å. These results suggest that the rhombohedral $BiFeO_3$ structure undergoes a monoclinic or a tetragonal distortion on doping, possibly associated with the $R3m$ space group, which involves Fe displacements relative to the cubic perovskite parent structure. Similar broadening in the neutron diffraction peaks has been observed in Mn-substituted $BiFeO_3$ ceramics, which has been attributed to anisotropic strain [21]. We do not expect any distortion at the Bi ions associated with transition metal doping at the Fe sites. Raman studies on Sc-doped $BiFeO_3$ have found no change in the Bi modes with up to 15% doping [17], suggesting that changes on the Fe site will not produce distortions at the Bi site. This is confirmed by our own Raman measurements on these samples (as discussed in the following).

The Raman spectra for the different samples are plotted in figure 2. The 20 μm beam size is significantly larger than the grain size, so these data show the response averaged over hundreds of crystallites. Group theory predicts a total of 13 $(4A_1 + 9E)$ Raman-active modes in the rhombohedral ($R3c$) $BiFeO_3$ crystal [22]. These modes have been observed in single crystals [23] and epitaxial thin films grown on (111) $SrTiO_3$ substrates [24]. We observe all the Raman-active modes with Raman shifts more than 160 cm^{-1}. We note that the A1(LO) mode associated with Bi shows no evidence for any shift, consistent with previous reports [17] that doping on the Fe site should not produce any structural distortion

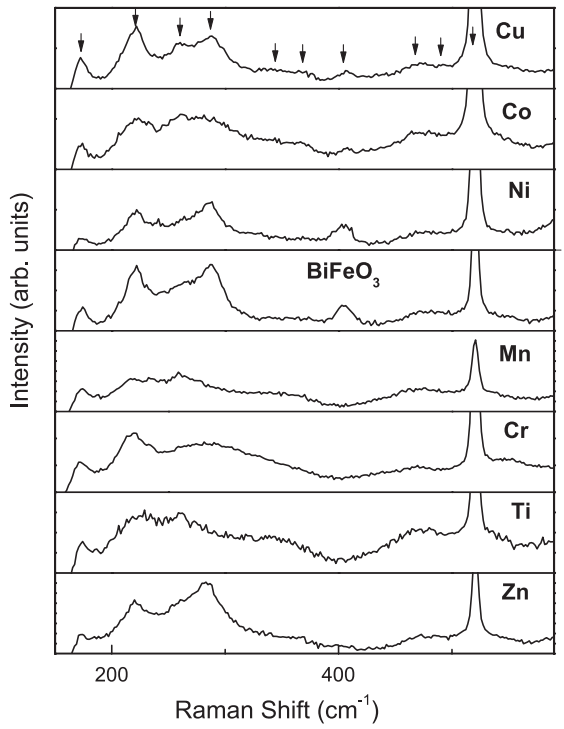

Figure 2. Room temperature Raman spectra of undoped and TM-ion-doped $BiFeO_3$. Arrows indicate the expected locations of the Raman-active modes. The large peak at 520 cm^{-1} arises from the silicon substrate. The label for each panel indicates the transition metal dopant added to each $BiFeO_3$ sample.

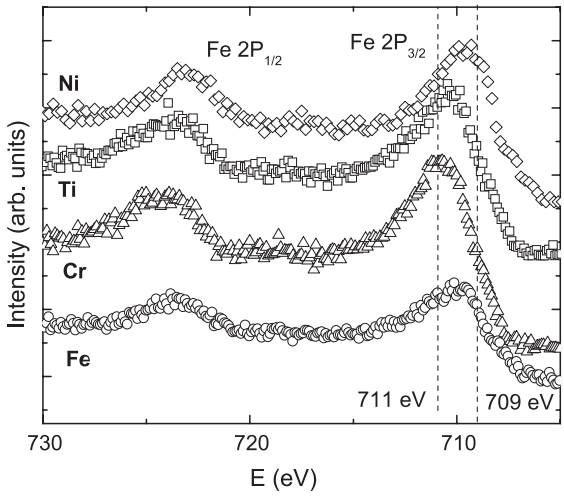

Figure 3. Fe XPS spectra for undoped $BiFeO_3$ (circles), Cr-doped $BiFeO_3$ (triangles), Ti-doped $BiFeO_3$ (squares) and Ni-doped $BiFeO_3$ (diamonds). The dashed lines indicate the approximate position of the Fe $2P_{\frac{3}{2}}$ peak for the 3+ valence (711 eV) and the 2+ valence (709 eV). The curves have been offset vertically for clarity.

about the Bi site. Further, as our films are prepared on silicon substrates, the strong silicon peak at 520 cm^{-1} masks the $BiFeO_3$ peak at ≈520 cm^{-1}. It is interesting to note that we observe the E(TO8) phonon at 404 cm^{-1} in $BiFeO_3$, close to the theoretically predicted value of 409 cm^{-1} [22], compared to 437 cm^{-1} observed in single crystals [23]. The principal change in the spectra that occurs upon TM ion doping is the shift in the 404 cm^{-1} mode. This mode vanishes when the films are doped with Mn, Cr, Ti and Zn whose ionic radii are larger than Fe, whereas the mode somewhat hardens on doping with Cu, Co and Ni, which have ionic radii smaller than that of Fe. Because the higher frequency Raman modes are generally associated with vibrational modes involving oxygen, these shifts in the E(TO8) mode could potentially be associated with rotation of the oxygen octahedra associated with the $R3c$ space group. We note that, although we cannot definitively identify the structural distortions giving rise to the changes in Raman spectra (figure 2) and XRD spectra (figure 1), these can in principle arise from completely different displacements.

Because the Fe valence is expected to play an important role in determining the magnetic and electrical properties of the films, we used XPS to directly measure the valence state of the Fe and dopant ions for several different samples including the Cr-, Ti- and Ni-doped films. XPS measurements at the dopant energies (not shown) established that the valence state of the Ni, Cr and Ti ions are 2+, 3+ and 4+, respectively, consistent with their valence in the precursor solution. Figure 3 shows the XPS spectra near the Fe edge for the undoped $BiFeO_3$ sample and for the Ni-, Cr- and Ti-doped films. We find that the Fe is predominantly in the 3+ valence state for the Cr, Ti and undoped films, with the $2P_{\frac{3}{2}}$ peak falling at 711 eV. For the Ni-doped sample this peak is shifted to lower energy levels, indicating some fraction of the Fe ions have a 2+ valence with the $2P_{\frac{3}{2}}$ peak at 709 eV. This observation is consistent with previous studies that have proposed that the Fe in $BiFeO_3$ films doped with Ti^{4+} is mainly in the 3+ state while samples doped with Ni^{2+} have some of the Fe in the 2+ state [15]. Although these XPS studies directly establish that the Fe valence in $BiFeO_3$ is sensitive to the valence of the dopant ion, for reasons discussed below we do not believe that the magnetic and electrical properties of our samples are mainly determined by this Fe valence.

Figure 4 shows the room temperature magnetic hysteresis curves for both the $BiFeO_3$ and TM-doped $BiFeO_3$ samples. There is a small increase in the saturation magnetization (M_s) of $BiFeO_3$ films with Ti, V, Mn, Cu and Zn doping, and a much larger increase with Cr, Co and Ni doping. The highest value of M_s (8.5 emu cm^{-3}) and coercive field H_c (173 Oe) occurs in the Cr-doped samples, with the Co-doped sample also showing relatively large values of M_s (7.5 emu cm^{-3}) and H_c (135 Oe). These results are different than those reported previously, which found that Co-doped $BiFeO_3$ films had coercivities of the order of $H_c = 2$ kOe at room temperature [21], with much smaller coercivities found for Cr-doped films. This discrepancy indicates that extraneous sample quality issues may have a significant effect on the magnetic properties of these transition-metal-doped films. Because large values of the saturation magnetization, of the order of 380 emu cm^{-3}, have been observed in epitaxial $BiFeO_3$ films containing γ-Fe_2O_3 impurities [25], we measured field-cooled (FC) and zero-field-cooled (ZFC) magnetization curves for the different samples to more carefully investigate the possible role played by magnetic impurities.

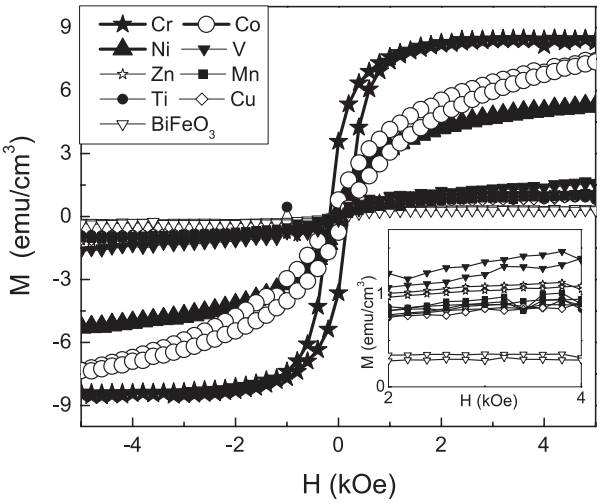

Figure 4. Magnetization versus magnetic field measured at 300 K for undoped and TM-doped samples. The $M(H)$ loops have been displayed in the order of increasing M_s values for undoped $BiFeO_3$ (open triangles) and Cu-(open diamonds), Ti-(filled circles), Mn-(filled squares), Zn-(open stars), V-(filled down triangles), Ni-(filled up triangles), Co-(open circles), and Cr-(filled stars) doped $BiFeO_3$ films, respectively. Inset: expanded view of bottom part of $M(H)$ loops near saturation.

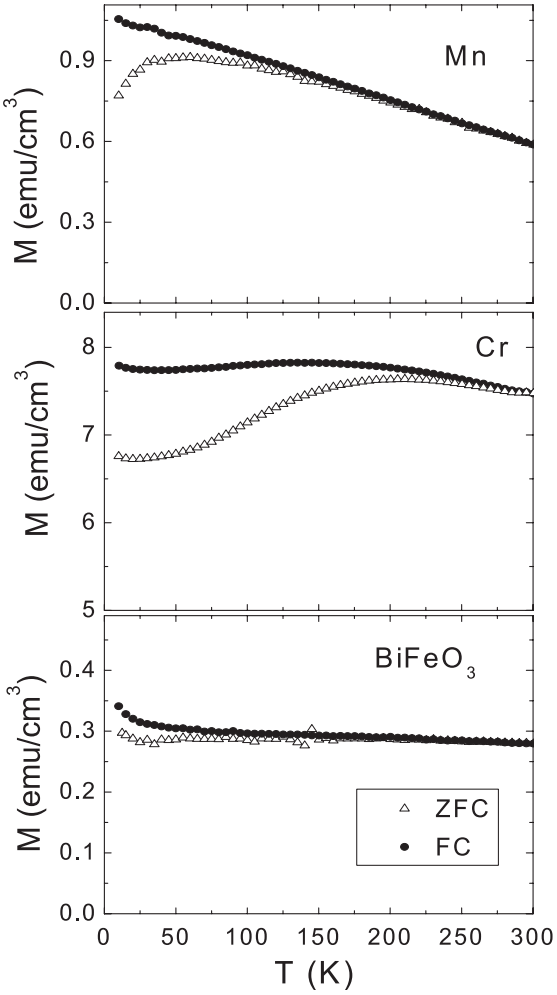

Figure 5. Field-cooled (FC)/zero-field-cooled (ZFC) magnetization curves for Mn-doped $BiFeO_3$ (upper panel), Cr-doped $BiFeO_3$ (middle panel) and undoped $BiFeO_3$ (lower panel). All data were measured on warming in a field of 1 kOe.

Representative ZFC/FC magnetization data are shown in figure 5; other films exhibit qualitatively similar behavior to the Mn- and Cr-doped samples with only the Zn- and Cu-doped films showing minimal FC–ZFC splitting. The $BiFeO_3$ magnetization curves are relatively flat, with a small Curie tail developing at low temperatures. The Mn and Cr curves show some splitting between the FC and ZFC curves together with a peak in the ZFC magnetization. This behavior is typical of superparamagnetic nanoparticles, and may be indicative of nanoscale magnetic secondary phases being present in these films. Although these data strongly suggest that impurity clusters may affect the magnetic properties of these TM-doped $BiFeO_3$ films, we do not believe they play a dominant role in determining the saturation magnetization for two reasons: (1) the ZFC curves do not tend towards $M = 0$ at $T = 0$, as one would expect if the impurity phases were the only contributions to the magnetization and (2) the size of the magnetic moment is significantly smaller than what has been measured previously in systems with iron oxide impurities [25].

We have investigated the electrical properties of the sample by measuring J–E and C–V curves and the charge density as a function of voltage at room temperature. In order to minimize the effects of pinholes seen in SEM images, we deposited a thin layer of Al_2O_3 on top of the films. For these measurements, the conducting silicon substrate was used as the bottom electrode and we evaporated a thin layer of gold on top of the Al_2O_3 to serve as the top electrode. We plot the J–E curves for these films in figure 6, with the exception of the Ni- and V-doped samples which are similar to the Cr-doped film, but are somewhat noisy and have been omitted for clarity. These films are rather leaky; significant current develops in most samples even with relatively modest applied voltages. Most of the films show rather low resistivity compared to the undoped $BiFeO_3$, with the Mn- and Zn-doped samples being particularly conducting. Only the Co-doped film shows even a modest reduction in the leakage current. These results on the electrical properties of TM-doped $BiFeO_3$ films again differ from previous reports, which found that the leakage current for Cr- and Mn-doped samples was smaller than for pure $BiFeO_3$ [18]. Because of the relatively high conductivity of these samples, it is difficult to extract a reliable estimate of the ferroelectric moment from polarization loops [26]. Nevertheless, in order to further qualitatively compare the electrical properties of the films, we measured the voltage-dependent remanent charge on the films using a Sawyer–Tower circuit, as shown in figure 7(a). While the undoped $BiFeO_3$ and Cr-doped $BiFeO_3$ films may show a hint of saturated ferroelectric behavior, these curves are principally indicative of lossy dielectric behavior. However, we also extracted the C–V curves from these P–E loops, as shown in figure 7(b). The butterfly structure of this C–V curve measured on undoped $BiFeO_3$ is consistent with this sample developing ferroelectric order [27].

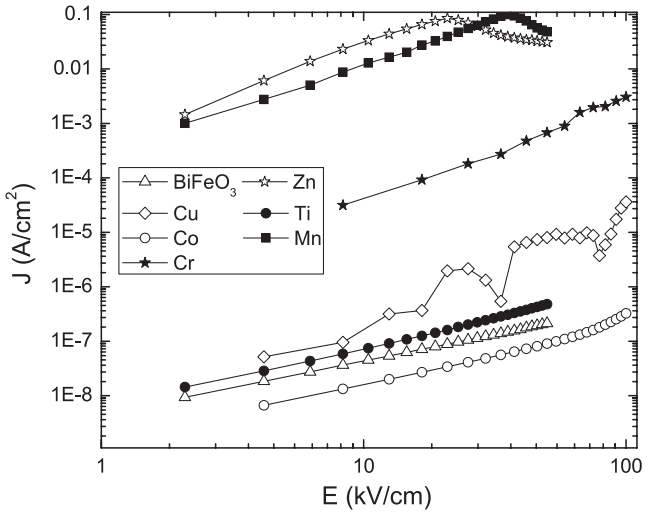

Figure 6. Room temperature J–E curves for the TM-doped $BiFeO_3$ films.

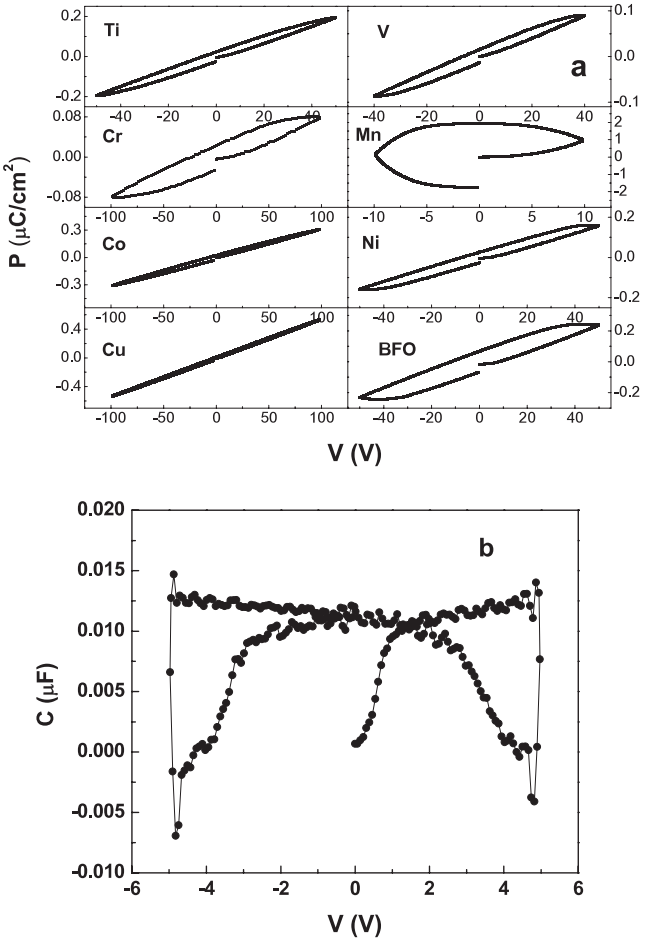

Figure 7. (a) Surface charge versus applied voltage for the TM-doped $BiFeO_3$ films. The label for each panel indicates the transition metal dopant added to each $BiFeO_3$ sample. (b) C–V characteristics of the undoped $BiFeO_3$ film.

Although one of the goals of this study was to determine the mechanisms through which the transition metal dopants modify the magnetic and electrical properties of $BiFeO_3$, the results are ambiguous. We do not find any evidence that Fe valence fluctuations are significantly affected by doping. Our XPS studies show that both the undoped films and Cr-doped films contain Fe in the 3+ state, and the leakage current (figure 6) does not appear to depend on the valence of the TM dopant ion. Furthermore, the magnetic properties (both saturation magnetization and coercivity) do not vary systematically with the local moment of the dopant ion. Cr- and Co-doped $BiFeO_3$ films show an improvement in the magnetic properties, but Ni- and Mn-doped films exhibit much smaller changes. Additionally, the temperature-dependent magnetization curves (figure 5) are history-dependent for many of the dopants, indicating that nanoscale impurity phases or structural defects may play a role in determining the magnetic properties of the films. Taken in aggregate, these results strongly suggest that the magnetic and electrical properties of polycrystalline TM-doped $BiFeO_3$ films are dominated by extrinsic effects including defects, grain boundaries, etc. Although intrinsic changes arising from structural distortions or valence effects may also be relevant for certain samples, we do not see any systematic variation in the multiferroic properties of $BiFeO_3$ with TM doping, suggesting that these intrinsic effects are negligible compared to extrinsic effects. This conclusion is strengthened by the observation that other studies on TM-doped $BiFeO_3$ films found qualitatively different behavior for nominally similar samples [18]. This emphasizes the fact that investigations on the properties of doped $BiFeO_3$ should be done on very high quality samples to minimize possible extrinsic effects.

4. Conclusion

In conclusion, we have successfully prepared single-phase $BiFeO_3$ and TM-doped $BiFeO_3$ thin films, some with a small amount of secondary phase, on conducting silicon substrates using a simple spin-coating technique. One specific Raman mode is suppressed on doping with larger transition metal ions, suggesting that there may be some symmetry breaking structural distortion in these samples. Investigation of magnetic properties indicates that Cr doping in $BiFeO_3$ substantially enhances the ferromagnetic moment but also has a small negative effect on the electrical properties of the samples. However, we did not observe any systematic dependence on atomic number/ion size of either magnetic or electrical properties with TM doping. This strongly suggests that extrinsic effects, including the presence of microstructural defects or grain boundaries, may be primarily responsible for determining the magnetic and electrical properties of doped polycrystalline $BiFeO_3$ samples.

Acknowledgments

This work has been supported by the NSF through DMR-0644823 and by the Institute for Manufacturing Research at Wayne State University.

References

[1] Fiebig M 2005 *J. Phys. D: Appl. Phys.* **38** R123
[2] Hill N A 2000 *J. Phys. Chem.* B **104** 6694
[3] Eerenstein W, Mathur N D and Scott J F 2006 *Nature* **442** 759
[4] Kimura T, Lawes G, Goto T, Tokura Y and Ramirez A P 2005 *Phys. Rev.* B **71** 224425
[5] Lawes G *et al* 2005 *Phys. Rev. Lett.* **95** 087205
[6] Zhao T *et al* 2006 *Nat. Mater.* **5** 823
[7] Wang J *et al* 2003 *Science* **229** 1719
[8] Palker V R, John J and Pinto R 2002 *Appl. Phys. Lett.* **80** 1628
[9] Uchida H, Ueno R, Funakubo H and Kodo S 2006 *J. Appl. Phys.* **100** 014106
[10] Kim J K, Kim S S, Kim W-J, Balla A S and Guo R 2006 *Appl. Phys. Lett.* **88** 132901
[11] Lee S U, Kim S S, Jo H K, Park M H, Kim J W and Bhalla Amar S 2007 *J. Appl. Phys.* **102** 044107
[12] Kim D H, Lee H N, Biegalski M D and Christen H M 2007 *Appl. Phys. Lett.* **91** 042906
[13] Hongri L and Yuxia S 2007 *J. Phys. D: Appl. Phys.* **40** 7530
[14] Kumar M and Yadav K L 2006 *J. Appl. Phys.* **100** 074111
[15] Qi X, Duo J, Tomov R, Blamire M and MacManus-Driscoll J 2005 *Appl. Phys. Lett.* **86** 062903
[16] Azuma M, Kanda H, Belik A A, Shimakawa Y and Takano M 2007 *J. Magn. Magn. Mater.* **310** 1177
[17] Yasui S, Uchida H, Nakai H, Nishida K, Funakubo H and Koda S 2007 *Appl. Phys. Lett.* **91** 022906
[18] Naganuma H, Miura J and Okamura S 2008 *Appl. Phys. Lett.* **93** 052901
[19] Kubel F and Schmid H 1990 *Acta Crystallogr.* **46** 698
[20] Selbach S M, Tybell T, Einarsrud M-A and Grande T 2008 *Adv. Mater.* **20** 3692
[21] Sosnowska I, Schafer W, Kockelmann W, Anderson K H and Troyanchuk I O 2002 *Appl. Phys.* A **74** S1040
[22] Hermet P, Goffinet M, Kreisel J and Ghosez Ph 2007 *Phys. Rev.* B **75** 220102
[23] Fukumara H, Matsui S, Harima H, Takahashi T, Itoh T, Kisoda K, Tamada M, Noguchi Y and Miyayama M 2007 *J. Phys.: Condens. Matter* **19** 365224
[24] Singh M K, Ryu S, Jang H M and Jo M-H 2006 *Appl. Phys. Lett.* **88** 042907
[25] Bea H *et al* 2005 *Appl. Phys. Lett.* **87** 072508
[26] Dawber M, Rabe K M and Scott J F 2005 *Rev. Mod. Phys.* **77** 1083
[27] Serrao C R *et al* 2005 *Phys. Rev.* B **72** 220101